



Research article

Ratiometric intracellular pH sensors based on nitrogen-doped graphene oxide quantum dots

Xiang Zhang^a, Yu Gu^a, Yun Zhang^c, Guo-Yin Yu^d, Zhi-Peng Liao^b, Hui-Fang Wu^b,
Chuan-Guo Shi^{b,d,*}^a Nantong Ecological Environment Monitoring Center, Nantong, 226007, PR China^b School of Chemistry and Chemical Engineering, Nantong University, Nantong, 226019, PR China^c Jiangsu Hydrometry and Water Resources Reconnaissance Bureau Nantong Branch Officer, Nantong, 2260006, PR China^d Jiangsu Grace-TECH Environmental Engineering Technology Company Limited, Nantong, 226602, PR China

ARTICLE INFO

Keywords:

Fluorescence

Graphene quantum dots

Optical sensing

ABSTRACT

Intracellular pH (pHi) is very essential for the function of cells and organisms. Thus, it is of great scientific and technical significance to develop nanosensors for probing pHi. In this work, nitrogen-doped graphene oxide quantum dots (N-GOQDs) with fluorescent efficiency of 54% are prepared. The fluorescent spectrum excited at 340 nm contains two remarkable bands at 430 and 520 nm. Interestingly, when pH value increases from 3.6 to 10.5, the blue band at 430 nm slightly changes, while the green band at 520 nm significantly quenches. The change of fluorescent intensities also can be reflected by the variation of fluorescent color. The dual-emissive N-GOQDs are developed as ratiometric fluorescent probes for pHi, which can avoid the influence of several deviations, such as probe concentration, optical path length, and detector efficiency. As a proof of concept, pHi of HeLa cells is monitored successfully. This work demonstrates the construction of nano-biosensors based on N-GOQDs with bright fluorescence, high-stability, and good biocompatibility.

1. Introduction

Intracellular pH (pHi) constantly affects the function of the cell from proliferation and metabolism to apoptosis [1, 2, 3]. The change of pH value sensitively modifies various cellular actions, such as adaptation of cellular volume, membrane polarity, signaling, and so on [4, 5, 6, 7]. The functional disorder of cell is often related with abnormal pH values in organelles because the structural stability of proteins are strongly dependent on the pHi. For instance, the unusually low pH values will denature proteins or activate enzymes [8]. Thus, the pHi is an important indicator of the human physiologic state. For example, cancer and Alzheimer's disease will lead to an abnormal pHi [9, 10]. Therefore, precisely monitoring on pH distribution and fluctuation in living cells with high temporal and spatial resolution is vital to the understanding of cellular processes, which will gain a deep insight into the physiological and pathological processes.

To date, a variety of techniques have been explored to detect the pHi, such as the utilization of H⁺ permeable microelectrodes, nuclear magnetic resonance (NMR), optical absorption spectroscopy, and fluorescence spectroscopy [7, 11, 12]. As well accepted, the optical signals can

be recorded at a high spatial and temporal resolution without direct contact. Thus, fluorescent technique based on pH-sensitive probes is a sensitive, convenient, and noninvasive method, which provides a powerful tool to measure the pHi of intact cells and subcellular regions. In particular, ratiometric sensors based on fluorophores with two emission peaks can avoid the interference of variations in the local probe concentration, temperature, and optical path length [13, 14, 15, 16, 17, 18]. In recent years, great efforts have been made to develop ratiometric fluorescent pH sensors [19, 20, 21, 22, 23, 24, 25]. For examples, fluorescent proteins and organic dyes have been extensively exploited for intracellular pH detection [19, 20, 21, 22, 23, 24, 25]. Nevertheless, these probes are facing severe limitations. In particular, the rapid photobleaching disallows continuous real-time tracking of cellular processes.

Recently, nanoparticle (NP) and quantum dot (QD)-based ratiometric pH sensors have attracted growing awareness due to their notable advantages [23, 24]. Up to now, a large number of fluorescent nanosensors based on silicon NP, polymers, QDs, InGaN-GaN nanowires and carbon dots have been gracefully designed to quantify intracellular pH [19, 20, 21, 22, 23, 24, 25, 26, 27, 28, 29, 30, 31, 32, 33, 34]. However, this type of sensors are usually composed of two components, i.e. a photostable

* Corresponding author.

E-mail address: shichuanguo@ntu.edu.cn (C.-G. Shi).

NP/QD and a pH-sensitive fluorescent protein/dye [19, 20, 21, 24, 25, 26, 27, 28]. The NPs/QDs in such sensors are just scaffolds to form the composite while the NPs/QDs themselves are insensitive to pH, thus do not take part in the fluorescent pH measurement. Moreover, limited by the large size or low biocompatibility, most of these composite sensors only can detect the pH value at a low spatial resolution. Therefore, the development of pH sensors with smaller size and higher biocompatibility will be highly desirable.

Nowadays, luminescent graphene oxide quantum dots (GOQDs) have attracted tremendous attention in the research community of physics, chemistry, materials science, and biology, because of their unique quantum effect caused by ultrasmall size, satisfactory stability, high photoluminescent quantum yield, low-cost, and negligible bio-toxicity [35, 36]. In addition, the oxygen related groups at the lateral sides are hydrophilic, which not only endow the GOQDs with good solubility but also facilitate the chemical modifications by different functional groups [37, 38, 39, 40]. The applications of GOQDs in biosensing, bio-tracing, drug delivery, light emitting devices, and solar cells have been demonstrated [41, 42]. In this work, nitrogen-doped GOQDs (N-GOQDs) were obtained by a facile solvothermal method. The fluorescence from N-GOQDs exhibits remarkable pH dependent feature. The intensity ratio between blue and green emissions increases as the pH value increases, which can be used to ratiometrically monitor pH value in bio-system. The good biocompatibility of the N-GOQDs is verified. And the monitoring of pHi of HeLa cells is then demonstrated.

2. Results and discussion

As illustrated in Figure 1a, the N-GOQDs were synthesized by using the GO micro-sheets with lateral sizes about several micrometers as the raw material. To dope nitrogen into GOQDs, the GO powder was dispersed into N,N-dimethylformamide (DMF). Then the GO-DMF suspension was treated in an autoclave at 200 °C for 24 h. DMF served as a source of nitrogen could be decomposed to dimethylamine and carbon

monoxide at such a high temperature. Then the decomposed dimethylamine bonded with the epoxy group on the GO to yield 1,2-amino alcohol via nucleophilic ring-opening reaction [43]. Figure 1b shows the transmission electron microscopy (TEM) image of the as-prepared N-GOQDs. Size distribution was acquired according to the TEM image (Figure 1c). The sizes of N-GOQDs mainly distribute in the range from 3 to 7 nm. The most probable size is about 5 nm. The ultrasmall size indicates an ultrahigh spatial resolution for biosensing, which also ensure the N-GOQDs enter the cells smoothly.

The doping of nitrogen into N-GOQDs is evidenced by X-ray photoelectron spectroscopy (XPS) results. The survey XPS spectrum of the N-GOQDs is shown in Figure 2a. Three main peaks related to C 1s, O 1s, and N 1s are noted. The corresponding content of each element is displayed in the table. The doping content of N element is about 8.2 at%. The C 1s, O 1s, and N 1s core XPS spectra are shown in Figure 2b-d, respectively. The C 1s spectrum includes three peaks, which are ascribed to C-C/C=C at 284.8 eV, C-O/CQO at 287.1 eV, and C=O at 289.3 eV, respectively (Figure 2b). The O 1s spectrum is divided to three sub-bands of C-O, C=O, and -OH (Figure 2c) [44]. The N 1s spectrum suggests the existence of three different nitrogen species, i.e. N-C, N-H, and N-O (Figure 2d). The main peak at 401.3 eV is attributed to the N-C bond of amino alcohol, indicating the binding between decomposed dimethylamine and aromatic ring of GOQDs [43].

The photoluminescence (PL) spectra of N-GOQDs aqueous solution are measured by changing the excitation wavelength (Figure 3a). The PL excitation (PLE) spectra relating to different emission wavelengths are shown in Figure 3b. As displayed in Figure 3a, when the excitation wavelength is increased, the fluorescent peak location gradually red-shifts, which is similar to the PL of undoped GOQDs. For GOQDs, all the PL spectra only exhibit a single peak as the excitation wavelength changes from 320 to 420 nm. Whereas, the PL spectra of N-GOQDs excited at 320–360 nm evidently contain two subpeaks. One fluorescent peak locating at about 430 nm is designated as FL1 and the other fluorescent peak appearing at 520 nm is designated as FL2. The FL1 peak has been

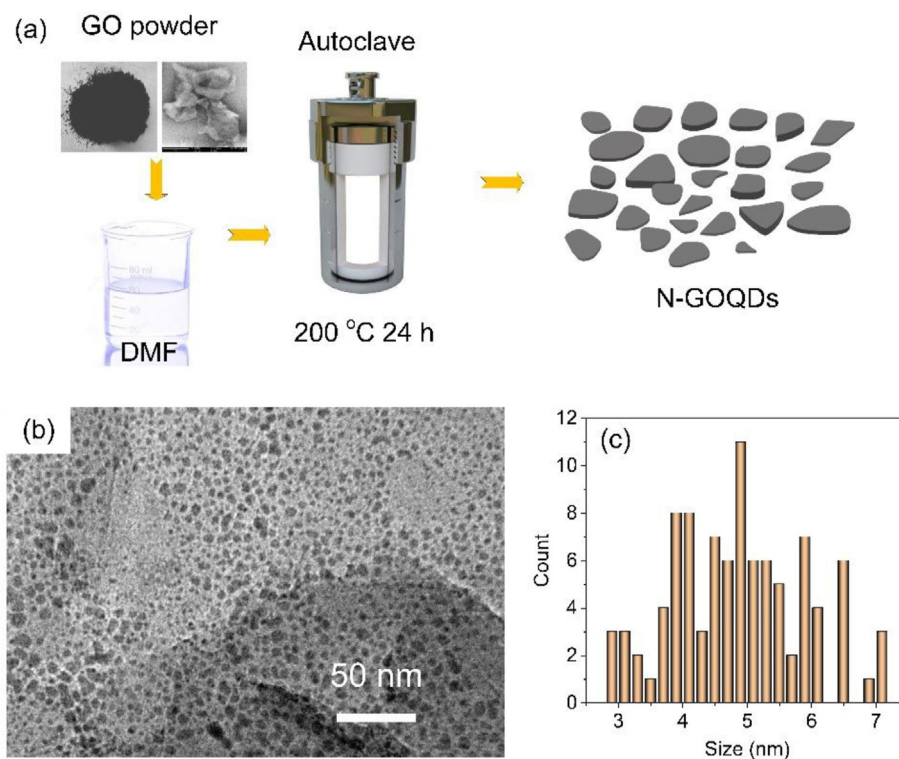


Figure 1. (a) Schematic illustration for the preparation of N-GOQDs. (b) TEM image of the N-GOQDs. (c) Size distribution of the N-GOQDs calculated from the TEM image.

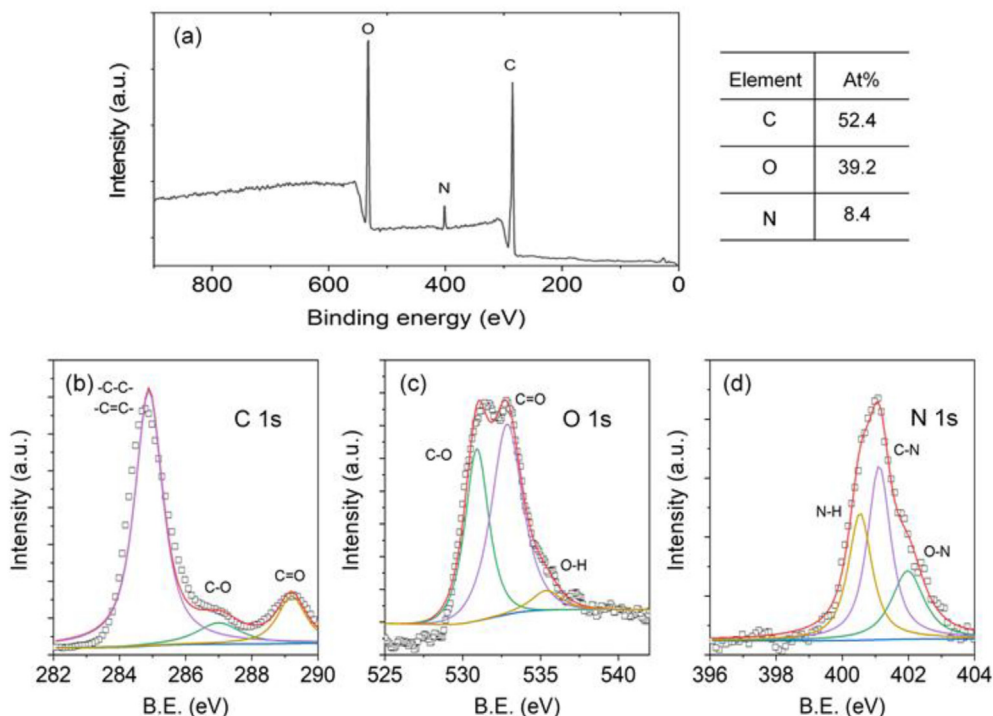


Figure 2. (a) XPS survey spectrum and elemental contents. C 1s (b), O 1s (c), and N 1s (d) core spectra of the N-GOQDs.

frequently observed in GOQDs, which is generally attributed to the size effect of sp^2 clusters [45]. The additional FL2 fluorescent peak is ascribed to the doped nitrogen. The dimethylamido is a strong electron-donating group, which leads to a red shift of fluorescence, consequently an additional PL band with longer emission wavelength is induced [43]. As shown in Figure 3b, the PLE spectra of N-GOQDs comprises three sub-bands. The two PLE bands at about 250 and 330 nm are caused by $\pi-\pi^*$ transitions of C=C and $n-\pi^*$ transitions of C=O, respectively, which also can be discerned in PLE of GOQDs [45, 46, 47]. The additional PLE band at 375 nm is caused by the doped nitrogen [45]. The fluorescent quantum yield (QY) of N-GOQDs solution is about 54%. The high fluorescent efficiency ensures the optical sensing based on N-GOQDs has a high signal-noise ratio and high accuracy.

To make a calibration between pH value and fluorescent intensity of N-GOQDs, the pH value of the cell medium is carefully changed by adding NaOH or HCl. Hepes is added in the cell medium to ensure pH stability during the measurements. Then the same amount of N-GOQDs is dispersed in cell media at a series of pH values. Fluorescence spectra from the media excited by a 340 nm monochromatic light is recorded. As

revealed in Figure 4a, all the fluorescence spectra constantly contain FL1 and FL2. When the pH value increases from 3.6 to 10.5, the intensity of FL1 changes little while FL2 remarkably quenches. Thus, as plotted in Figure 4b, the intensity ratio between FL1 and FL2 bands (defined as R) monotonously increases with environmental pH value. The ratio slightly changes in the acid conditions (pH = 3~7) then significantly increases in the pH range of 7~11, suggesting the variation of physiological pH at weak alkalinity can be sensitively monitored by the fluorescence of N-GOQDs. To quantitatively determine the pH values, the experimental results are fitted by the following Eq. (1),

$$\text{pH} = 8.89124 + 0.5435 \ln \left(\frac{1.45538}{2.2727 - R} - 1 \right) \quad (1)$$

Therefore, the pH of an unknown environment can be detected by the R value. As shown in the inset of Figure 4b, this pH dependent behavior of fluorescence can be highlighted by the color change. At a low pH value of 3.6, the color of the solution was dominated by the green emission at 520 nm. Whereas, the color of the solution becomes blue due to the dominant fluorescence at 440 nm when the pH increases to 10.5.

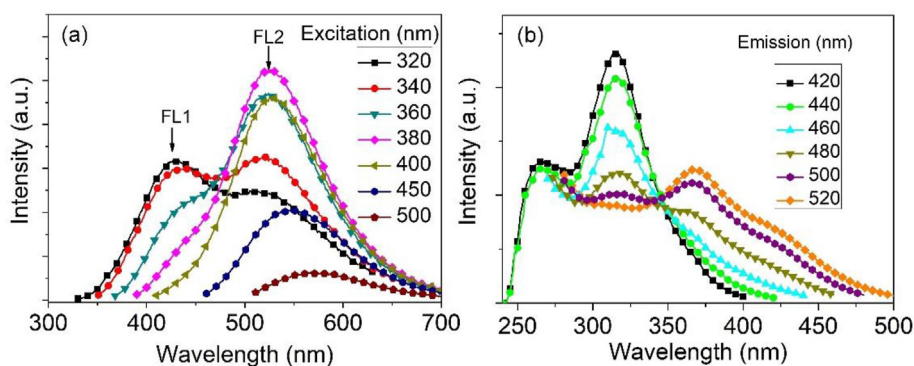


Figure 3. (a) PL spectra of the N-GOQDs aqueous solution. The excitation wavelength is changed from 320 to 500 nm. (b) PLE spectra of the N-GOQDs aqueous solution measured at different emission wavelengths.

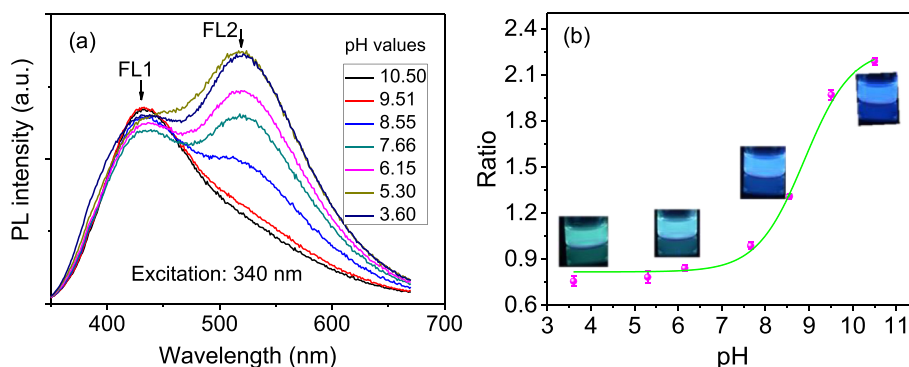


Figure 4. (a) PL spectra of the N-GOQDs in culture media at different pH values. A 340 nm UV monochromatic light was used as the excitation source. (b) The intensity ratio between FL1 and FL2 bands is plotted as a function of pH value. Inset: Photographs of the N-GOQDs in culture media with the different pH values under irradiation of a 365 nm UV lamp.

Before the measurements of intracellular pH, the reliability and accuracy of pH sensing by fluorescence of the N-GOQDs are examined. Unknown quantities of NaOH or HCl are randomly added into a culture medium containing the N-GOQDs. PL spectra are measured at each step as indicated by the order number (Figure 5a). The intensity ratios between FL1 and FL2 bands at each step are plotted in Figure 5b. When NaOH is added, the intensity ratio increases. Whereas, when HCl is added, the intensity ratio decreases. The observation is consistent with the relationship shown in Figure 4b. As shown in Figure 5c, the pH values of the unknown experiments are determined by Eq. (1). To validate the fluorescent method, the pH values are also comparatively tested by a commercial pH meter. As compared in Figure 5c, the pH values determined by the two different methods are very close, indicating fluorescent method developed in this work is accurate and reliable. The accuracy is defined as $A = 1 - \frac{|V_M - V_R|}{V_R}$, where V_M is the pH value measured by the fluorescent sensor and V_R is the real pH value. As shown in Figure 4d, the accuracy is generally higher than 0.97, which is a very competitive performance.

To demonstrate the applicability of N-GOQDs for intracellular pH monitoring, the pH_i value of HeLa cell is detected as an example. As shown in Figure 6a, bright field microscopic image after incubation with N-GOQDs shows the clear outlines of the living cells. Figure 6b shows a fluorescent micrograph of the HeLa cells incorporated with N-GOQDs excited by the 340 nm UV light. As shown by the bright spots, fluorescence of N-GOQDs is observed. Figure 6c displays the merged image of Figure 6a,b, demonstrating that N-GOQDs are distributed in the HeLa cells. A standard MTT assay (MTT = 3-(4,5-dimethylthiazol-2-yl)-2,5-diphenyl-tetrazolium bromide) was carried out to evaluate the cytotoxicity of the N-GOQDs. The viabilities of HeLa cells were tested after being incubated with N-GOQDs at different concentrations. As shown in Figure 6d, the cell viability exhibits a negligible deterioration after treatment with the N-GOQDs at a concentration of up to 60 μg/mL, undoubtedly indicating the N-GOQDs are bio-compatible.

To determine the pH_i of HeLa cells, fluorescence spectrum of HeLa cells incorporated with N-GOQDs was measured. The fluorescent microscopic image suggests no fluorescence is observed from the cell medium. Moreover, to ensure the detected fluorescence is mainly from

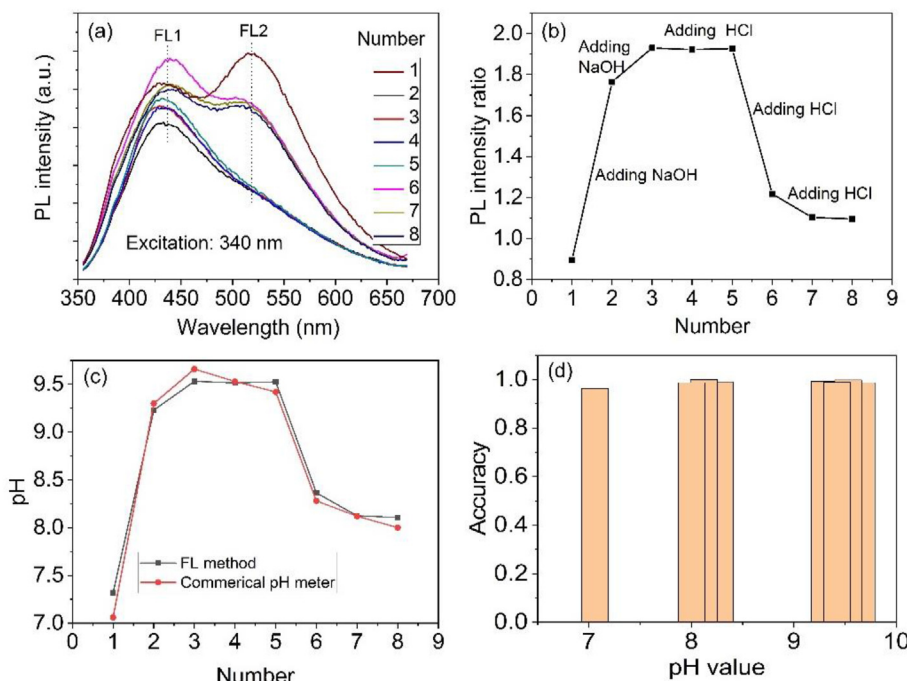


Figure 5. (a) Fluorescent spectra acquired from culture media containing N-GOQDs at unknown pH. (b) Plots of the FL1/FL2 intensity ratios corresponding to panel (a). (c) Comparison of pH values measured by the fluorescence of N-GOQDs (black) and a commercial pH meter (red). (d) Accuracy of the pH sensing by N-GOQDs.

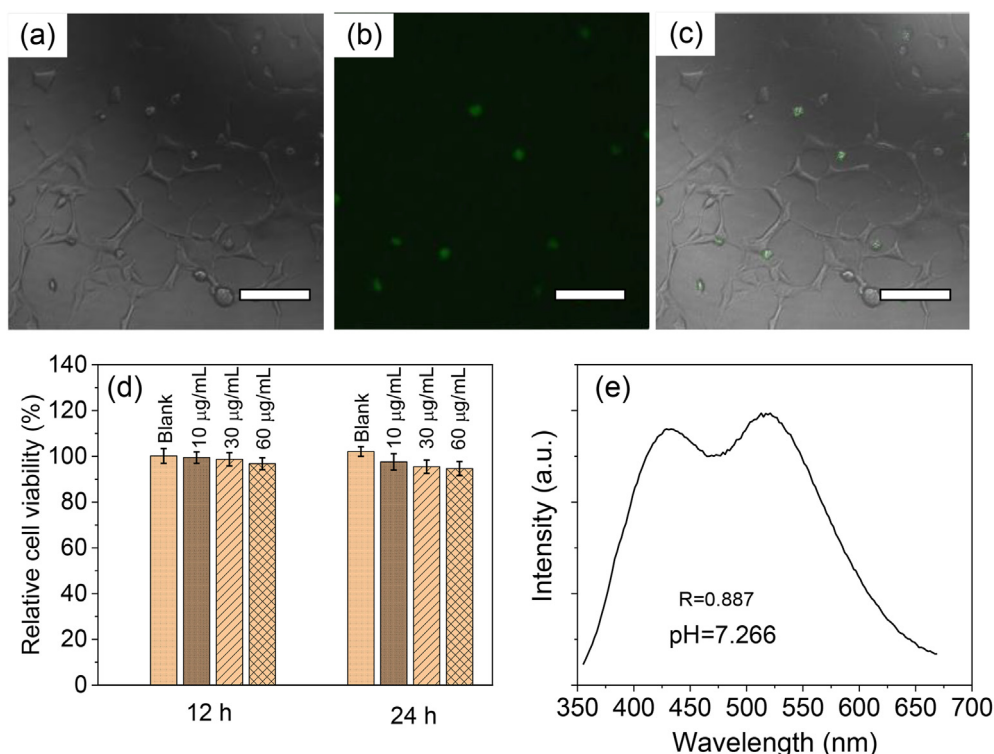


Figure 6. Cell imaging under bright field (a) and 365 nm UV excitation (b). (c) The merged image of panel (a) and panel (b). All scale bars are 100 µm. (d) Cell viability after incubation with N-GOQDs for 12 and 24 h. (e) Fluorescent spectrum of N-GOQDs within normal HeLa cells excited at 340 nm.

intracellular N-GOQDs, the HeLa cells were washed with phosphate buffer solution (PBS) to remove the residual extracellular N-GOQDs. Therefore, the detected fluorescent signal indeed comes from the intracellular N-GOQDs. The fluorescence spectrum is plotted in Figure 6e. According to the relationship presented in Figure 4b, the averaged pHi of HeLa cell is determined to be 7.266, which is in good agreement with the pHi of HeLa cell detected by other methods (7.2–7.4) [24]. In addition, there is a negligible photobleaching after continuous irradiation, indicating these N-GOQDs are highly photostable. Thus, these fluorescent N-GOQDs are very promising for applications in vivo imaging and biosensors.

3. Conclusion

In summary, highly fluorescent N-GOQDs were prepared by a solvothermal treatment of GO in DMF. The fluorescence spectrum excited at 340 nm contains two noticeable bands at 430 nm and 520 nm. The 520 nm-FL2 band is introduced by the doping of nitrogen. We found that the 430 nm-FL1 band changes slightly while the FL2 band remarkably quenches when pH value increases from 3.6 to 10.5. Therefore, the intensity ratio between FL1 and FL2 bands monotonously increases with environmental pH value, indicating pH can be easily monitored by reading out the fluorescent intensities. These fluorescent probes are suitable for a wide range of intracellular pH-dependent imaging applications. As a demonstration, pHi of HeLa cells is probed successfully. Therefore, the fluorescent N-GOQDs with high-stability and low-toxicity are developed as promising biosensors for practical applications.

4. Experimental section

Synthesis of N-GOQDs: A modified Hummer's method was used to prepare graphene oxide powder [48]. Concentrated H₂SO₄ (360 mL) and H₃PO₄ (40 mL) were added to a mixture of graphite powder (3.0 g) and KMnO₄ (18.0 g) under stirring. Then, the mixture was heated to 50 °C for 12 h. After it was cooled to room temperature, the mixture was subsequently poured onto ice (~400 mL) with hydrogen peroxide (3 mL). After

the reaction, the supernatant was dropped while the solid was collected after washing. Aqueous solution of the N-GOQDs was fabricated by a solvothermal process. Firstly, 80 mg GO were dispersed in 80 mL DMF by an ultrasonic treatment. Then NaOH was added to adjust pH of the GO solution to 7. The suspension was then transferred to a Teflon lined autoclave (100 mL), which was heated to 200 °C for 24 h. After that, the obtained suspension was treated by ultrasonic vibration for 1 h. The N-GOQDs solution was collected by centrifugation at 9000 rpm for 20 min. The N-GOQDs solution was then dialyzed in a dialysis bag with a molecular weight cut-off of 3500 Da for one day to remove the residual reactants. The solvent was removed by vacuum-rotary evaporation. Finally, N-GOQDs were dispersed in deionized water.

Characterizations: A JEOL-2100F transmission electron microscopy was used to capture TEM images. XPS results were obtained on a PHI 5000 Versa Probe. PL and time-resolved PL were measured on an Edinburgh FLS-920 spectrometer. Microscopic images were captured using an Olympus IX-71 microscope. The fluorescence of N-GOQDs was excited with a 375 nm UV light, which was obtained by a bandpass filter. Emission was collected with a 400 nm long-pass filter. The fluorescence quantum yield was measured by an absolute method, which is defined as the ratio between number of emitted photons and absorbed photons. The number of photons was measured by an integrating sphere equipped on a FluoroMax-4 spectrometer.

Cytotoxicity evaluation: The MTT assay was conducted to evaluate the relative cytotoxicity of the N-GOQDs. The HeLa cells were seeded on 96-well culture plates and allowed to attach overnight. Afterward, the indicated concentrations of N-GOQDs were added. The cells were incubated at 37 °C for 12 or 24 h. Then 20 µL of 5 mg/mL MTT solution in PBS was added to each well and incubated for an additional 4 h under 5% CO₂. After incubation, the supernatants were cautiously removed. Then to dissolve the formazan product, 200 µL DMSO was added into each well. An ELISA plate reader was used to measure the absorbance at 570 nm of each well. The reference wavelength was 630 nm.

Intracellular pH measurement by N-GOQDs: HeLa cells were incubated with N-GOQDs in medium at 37 °C for 1.5 h. The cells were then collected

by centrifugation at 2000 rpm and washed thrice with PBS. After that, the HeLa cells were dispersed in PBS buffer for PL measurements.

Declarations

Author contribution statement

Guo-Yin Yu: Performed the experiments; Analyzed and interpreted the data; Contributed reagents, materials, analysis tools or data; wrote the paper.

Zhi-Peng Liao: Performed the experiments; Contributed reagents, materials, analysis tools or data.

Hui-Fang Wu: Performed the experiments.

Chuan-Guo Shi: Conceived and designed the experiments; Analyzed and interpreted the data; Contributed reagents, materials, analysis tools or data; Wrote the paper.

Funding statement

This work was supported by National Natural Science Foundation of China (21375067 and 22106076), Nantong Science and Technology Project (MS12021052) and Jiangsu Industry University Research Cooperation Project (BY2021330).

Data availability statement

Data will be made available on request.

Declaration of interests statement

The authors declare no conflict of interest.

Additional information

No additional information is available for this paper.

References

- [1] I. Yuli, A. Oplatka, *Science* 235 (1987) 340.
- [2] M. Huang, X. Liang, Z. Zhang, J. Wang, Y. Fei, J. Ma, S. Qu, L. Mi, *Nanomaterials* 10 (2020) 604.
- [3] F.R. Maxfield, T.E. McGraw, *Nat. Rev. Mol. Cell Biol.* 5 (2004) 121.
- [4] J.R. Casey, S. Grinstein, J. Orłowski, *Nat. Rev. Mol. Cell Biol.* 11 (2010) 50.
- [5] W.B. Busa, R. Nuccitelli, *Am. J. Physiol.* 246 (1984) R409.
- [6] A. Jaworska, K. Malek, A. Kudelski, *Spectrochim. Acta A.* 251 (2021) 119410.
- [7] F.B. Loiselle, J.R. Casey, *Methods Mol. Biol.* 227 (2003) 259.
- [8] J. Han, K. Burgess, *Chem. Rev.* 110 (2010) 2709.
- [9] H. Izumi, T. Torigoe, H. Ishiguchi, H. Uramoto, Y. Yoshida, M. Tanabe, T. Ise, T. Murakami, T. Yoshida, M. Nomoto, K. Kohno, *Cancer Treat. Rev.* 29 (2003) 541.
- [10] T.A. Davies, R.E. Fine, R.J. Johnson, C.A. Levesque, W.H. Rathbun, K.F. Seetoo, S.J. Smith, G. Strohmeier, L. Volicer, L. Delva, E.R. Simons, *Biochem. Biophys. Res. Commun.* 194 (1993) 537.
- [11] S. Wray, *Am. J. Physiol.* 254 (1988) C213–C225.
- [12] T. Liu, J. Hu, Z. Jin, F. Jin, S. Liu, *Adv. Healthcare Mater.* 2 (2013) 1576.
- [13] T. Myochin, K. Kiyose, K. Hanaoka, H. Kojima, T. Terai, T. Nagano, *J. Am. Chem. Soc.* 133 (2011) 3401.
- [14] J.Y. Han, A. Loudet, R. Barhoumi, R.C. Burghardt, K. Burgess, *J. Am. Chem. Soc.* 131 (2009) 1642.
- [15] E. Nakata, Y. Yukimachi, Y. Nazumi, Y. Uto, H. Maezawa, T. Hashimoto, Y. Okamoto, H. Hori, *Chem. Commun.* 46 (2010) 3526.
- [16] M. Tantama, Y.P. Hung, G. Yellen, *J. Am. Chem. Soc.* 133 (2011) 10034.
- [17] R.L. Grant, D. Acosta, *In Vitro Cell. Dev. Biol. Anim.* 33 (1997) 256.
- [18] Z. Gan, Y. Hao, Y. Shan, *ChemNanoMat* 2 (2016) 171.
- [19] M. Wei, Y. Gao, X. Li, M.J. Serpe, *Polym. Chem.* 8 (2017) 127.
- [20] Y. Bao, H. De Keersmaecker, S. Corneille, F. Yu, H. Mizuno, G. Zhang, J. Hofkens, B. Mendrek, A. Kowalczyk, M. Smet, *Chem. Mater.* 27 (2015) 3450.
- [21] K. Paek, H. Yang, J. Lee, J. Park, B.J. Kim, *ACS Nano* 8 (2014) 2848.
- [22] B. Kong, A. Zhu, C. Ding, X. Zhao, B. Li, Y. Tian, *Adv. Mater.* 24 (2012) 5844.
- [23] J. Guo, S. Xiong, X. Wu, J. Shen, Paul K. Chu, *Biomaterials* 34 (2013) 9183.
- [24] X. Wang, Y. Feng, J. Liu, K. Cheng, Y. Liu, W. Yang, H. Zhang, H. Peng, *Spectrochim. Acta A.* 267 (2022) 120477.
- [25] I.L. Medintz, M.H. Stewart, S.A. Trammell, K. Susumu, J.B. Delehanty, B.C. Mei, J.S. Melinger, J.B. Blanco-Canosa, P.E. Dawson, H. Mattoussi, *Nat. Mater.* 9 (2010) 676.
- [26] W. Jens, T. Jorg, F. Florian, M.H. Detlev, E. Martin, *Nano Lett.* 12 (2013) 6180.
- [27] A.M. Dennis, W.J. Rhee, D. Sotto, S.N. Dublin, G. Bao, *ACS Nano* 6 (2012) 2917.
- [28] W. Shi, X. Li, H. Ma, *Angew. Chem. Int. Ed.* 51 (2012) 6432.
- [29] S.Q. Wu, Z. Li, J.H. Han, S.F. Han, *Chem. Commun.* 47 (2011) 11276.
- [30] W.J. Wang, J.M. Xia, J. Feng, M.Q. He, M.L. Chen, J.H. Wang, *J. Mater. Chem. B* 4 (2016) 7130.
- [31] A.O. Silva, M.O. Rodrigues, M.H. Sousa, A.F.C. Campos, *Colloid. Surface.* 621 (2021) 126578.
- [32] Z. Zhu, C. Liu, X.M. Song, Q. Mao, T. Ma, *ACS Appl. Bio Mater.* 4 (4) (2021) 3623.
- [33] X. Liu, J. Liu, B. Zheng, L. Yan, J. Dai, Z. Zhuang, J. Du, Y. Guo, D. Xiao, *New J. Chem.* 41 (2017) 10607.
- [34] L. Shen, C. Hou, J. Li, X. Wang, Y. Zhao, H. Yang, S. Yang, M. Yang, X. Luo, D. Huo, *Anal. Methods* 11 (2019) 5711.
- [35] Z. Gan, S. Xiong, X. Wu, C. He, J. Shen, P.K. Chu, *Nano Lett.* 11 (2011) 3951.
- [36] Z. Gan, H. Xu, Y. Hao, *Nanoscale* 8 (2016) 7794.
- [37] X. Zhu, J. Yu, Y. Yan, W. Song, X. Hai, *Talanta* 236 (2022) 122874.
- [38] P.H. Luo, Z. Ji, C. Li, G. Shi, *Nanoscale* 5 (2013) 7361.
- [39] K.J. Goswami, B. Gogoi, N.S. Sarma, *Sensor. Actuator. B Chem.* 350 (2022) 130892.
- [40] J. Shen, Y. Zhu, X. Yang, J. Zong, J. Zhang, C. Li, *New J. Chem.* 36 (2012) 97.
- [41] Z. Zhang, J. Zhang, N. Chen, L. Qu, *Energy Environ. Sci.* 5 (2012) 8869.
- [42] S. Zhu, S. Tang, J. Zhang, B. Yang, *Chem. Commun.* 48 (2012) 4527.
- [43] Q. Liu, B. Guo, Z. Rao, B. Zhang, J.R. Gong, *Nano Lett.* 13 (2013) 2436.
- [44] Z. Gan, L. Liu, L. Wang, G. Luo, C. Mo, C. Chang, *Phys. Chem. Chem. Phys.* 20 (2018) 18089.
- [45] Z. Gan, S. Xiong, X. Wu, T. Xu, X. Zhu, X. Gan, J. Guo, J. Shen, L. Sun, P.K. Chu, *Adv. Opt. Mater.* 1 (2013) 926.
- [46] G. Eda, Y.Y. Lin, C. Mattevi, H. Yamaguchi, H.A. Chen, I.S. Chen, C.W. Chen, M. Chhowalla, *Adv. Mater.* 22 (2010) 50.
- [47] M. Zhang, L.L. Bai, W.H. Shang, W.J. Xie, H. Ma, Y.Y. Fu, D.C. Fang, H. Sun, L.Z. Fan, M. Han, C.M. Liu, S.H. Yang, *J. Mater. Chem.* 22 (2012) 7461.
- [48] D.C. Marcano, D.V. Kosynkin, J.M. Berlin, A. Sinitskii, Z. Sun, A. Slesarev, L.B. Alemany, W. Lu, J.M. Tour, *ACS Nano* 4 (8) (2010) 4806.